Research Article Vol. 8, No. 4 / April 2020 / Photonics Research 475

PHOTONICS Research

Self-accelerated optical activity in free space induced by the Gouy phase

PENG LI,[1,3] XINHAO FAN,[1] DONGJING WU,[1] SHENG LIU,[1] YU LI,[1,2] AND JIANLIN ZHAO[1,4]

[1]MOE Key Laboratory of Material Physics and Chemistry under Extraordinary Conditions, and Shaanxi Key Laboratory of Optical Information Technology, School of Physical Science and Technology, Northwestern Polytechnical University, Xi'an 710129, China
[2]Northwestern Polytechnical University Ming De College, Xi'an 710124, China
[3]e-mail: pengli@nwpu.edu.cn
[4]e-mail: jlzhao@nwpu.edu.cn

Received 18 October 2019; revised 24 December 2019; accepted 15 January 2020; posted 16 January 2020 (Doc. ID 380675); published 23 March 2020

Optical activity (OA) is the rotation of the polarization orientation of the linearly polarized light as it travels through certain materials that are of mirror asymmetry, including gases or solutions of chiral molecules such as sugars and proteins, as well as metamaterials. The necessary condition for achieving OA is the birefringence of two circular polarizations in material. Here, we propose a new kind of self-accelerated OA in free space, based on the intrinsic Gouy phase induced mode birefringence of two kinds of quasi-non-diffracting beams. We provide a detailed insight into this kind of self-accelerated OA by analyzing angular parameters, including angular direction, velocity, acceleration, and even the polarization transformation trajectory. As the Gouy phase exists for any wave, this kind of self-accelerated OA can be implemented in other waves beyond optics, from acoustic and elastic waves to matter waves. © 2020 Chinese Laser Press

https://doi.org/10.1364/PRJ.380675

1. INTRODUCTION

Optical activity (OA) was first observed in 1811 when plane-polarized light passing through quartz, manifested itself as the rotation of the orientation of linear polarization. Soon afterwards, various materials demonstrated optically active capability, such as sugars, proteins, gases, solutions, and solids that consist of chiral molecules, and even artificial materials [1,2]. Fundamentally, OA is a result of circular birefringence, as the right- and left-handed circular polarizations have different phase velocities because of the interaction between light and chiral molecules. Therefore, the rotation of the polarization plane is dependent on the chiral birefringence of molecules, i.e., the refractive index difference Δn of two circularly polarized components. Moreover, it is directly proportional to the path length through the substance. However, because of the dependence of molecular chirality, this typically physical phenomenon occurs only in chiral materials, which greatly limits its practical application.

In recent years, vector beams, which have spatially structured polarizations, have invoked interest in the scientific community due to their intriguing polarization properties [3–11]. Remarkably, based on various spatial modulation techniques, some vector beams with a longitudinally variant state of polarization have been proposed and demonstrated their analogous OA phenomena in free space [12–16]; for instance, the polarization oscillating beams resulting from the longitudinal intensity modulation [13], and vector Bessel beams with longitudinally varying polarization based on the modulation of transverse polarization structures [15,16]. Substantially, these active phenomena in free space are the result of the mode difference between Bessel beams with various longitudinal wave vectors, i.e., the mode birefringence [17]. However, for the Bessel beams, this mode birefringence induces an inevitable problem that two components with opposite circular polarizations have distinct intensity profiles, whose difference increases with the birefringence [18]. Furthermore, this linearly accumulated birefringence can only induce linear OA in free space.

In this paper, we propose a new kind of self-accelerated OA in free space based on the Gouy phases of two kinds of quasi-non-diffracting beams. The distinct Gouy phases of Laguerre–Gaussian (LG) beams with high-radial-order and profile-equivalent Bessel beams induce z-dependent mode birefringence, resulting in self-accelerated OA in free space. We provide a detailed insight into this kind of self-accelerated OA by demonstrating the controllability of rotation direction, angular velocity, and acceleration. Moreover, from a fundamental point of view, the intrinsic property of the Gouy phase indicates that this type of OA can be implemented to any wave beyond optics, ranging from other electromagnetic waves to matter waves [19–21].

2. THEORETICAL PRINCIPLE

The prior consideration of the OA is that the beam should sustain its profile upon polarization transformation, i.e., the mode stability. Considering the evolution properties of beams that have been reported, the non-diffracting beam understandably is the best candidate. However, as mentioned above, two Bessel beams used to generate OA have distinct intensity profiles. Therefore, we propose other spatially structured modes with a radially variant amplitude profile on the basis of transverse intensity consideration, e.g., the LG mode with large radial index. The LG beam was well known as its intrinsic orbital angular momentum (OAM) is associated with spiral phase [22] (characterized by the topological charge l). Currently, the radial index has demonstrated the significant influence on the beam propagation as an LG beam with a high radial order ($p \gg 1$) exhibits quasi-non-diffraction property in free space [23].

The LG mode solution of the Helmholtz function can be expressed as

$$E_{\mathrm{LG}}(r,\varphi,z) = \sqrt{\frac{2p!}{\pi(p+|l|)!}}\frac{1}{w(z)}\left[\frac{\sqrt{2}r}{w(z)}\right]^{|l|} L_p^{|l|}\left[\frac{2r^2}{w^2(z)}\right] \cdot \exp\left[-\frac{r^2}{w^2(z)}\right]\exp\left[i\frac{kr^2}{2R(z)}\right] \cdot \exp(-i\Phi)\exp(il\varphi)\exp(ikz), \tag{1}$$

where (r,φ,z) are the cylindrical coordinates; $L_p^{|l|}(\cdot)$ is the Laguerre polynomials; p and l are the radial and azimuthal indices, respectively; $\Phi = (2p+|l|+1)\arctan(z/z_R)$ denotes the Gouy phase; $R(z) = z[1+(z_R/z)^2]$ and $w(z) = w_0$ are the curvature and waist radii, respectively; and $z_R = kw_0^2/2$ is the Rayleigh length. For an LG mode with high radial order, i.e., $p \gg 1$, the Laguerre polynomial and Gaussian exponential term can be represented by the Bessel and Γ polynomials as [23]

$$\exp\left[-\frac{r^2}{w^2(z)}\right]\left[\frac{\sqrt{2}r}{w(z)}\right]^{|l|} L_p^{|l|}\left[\frac{2r^2}{w^2(z)}\right] \approx \frac{\Gamma(p+|l|+1)}{p!N^{|l|/2}} J_l\left[2\sqrt{2N}\frac{r}{w(z)}\right], \tag{2}$$

with $N = p + (|l|+1)/2$. Thus, the LG field can be rewritten as

$$E_{\mathrm{LG}}(r,\varphi,z) \propto J_l[k_r(p,l)r]\exp\left[i\frac{kr^2}{2R(z)}\right] \cdot \exp(-i\Phi)\exp(il\varphi)\exp(ikz), \tag{3}$$

where $J_l(\cdot)$ denotes the lth-order Bessel function of the first kind, $k_r(p,l) = 2/w(z)$ is the equivalent transverse wave vector of the Bessel field, and $R_0 = w_0$ is the effective radius of the LG field. Remarkably, the LG field presents amplitude profile exactly similar to a Bessel field, which has a transverse wave vector dependent on the radial and azimuthal indices of the corresponding LG field. To ensure the intensity similarity, in practice we first select indices of l and p and then calculate the parameters N and k_r to determine the Bessel beam intensity pattern.

Figures 1(a)–1(d) display the intensity distributions of the LG_{15}^0 and LG_{15}^1 beams, as well as their corresponding zeroth- ($l = 0$) and first-order ($l = 1$) Bessel beams without apodization, respectively. Figures 1(e) and 1(f) show the comparisons of intensity distributions along the radial direction. We can find that the inner rings (denoted by radial order p') of the LG beams, whose radial order is below $p/2$, i.e., $p' < p/2$, have identical intensity profiles with the Bessel beams. This elucidates that the coaxially superimposed field of such two kinds of beams has homogeneous polarization in such a region. More importantly, higher-radial-order LG beams have demonstrated the capability of quasi-non-diffracting and self-healing within the same region that belongs to the corresponding Bessel beam [23]. This means that the superimposed field can keep well the homogeneous polarization state in a certain longitudinal interval.

Besides the unique amplitude profiles, another characteristic associated with the transverse confinement of structured beams is the Gouy phase shift [24–27], which exists for any wave and accumulates with wave propagation according to specific function. The dependence of the Gouy phase on the spatial mode has induced some intriguing physical phenomena, such as lateral spin transport [28], polarization transition of focused vector vortex beams [29,30], and Gouy rotation of focused non-relativistic electron vortex beams [19]. Here, although the LG beam and its corresponding Bessel beam present similar amplitude profiles, their Gouy phases are distinctly different. The Gouy phase of the LG beam strongly depends on the azimuthal and radial indices simultaneously. The relationship is described in Eq. (1), i.e., $\Phi_{\mathrm{LG}} = (2p+|l|+1)\arctan(z/z_R)$ [31], where $z = 0$ corresponds to the position of the Gaussian beam waist. While the Gouy phase of the Bessel beam only depends on the transverse wave vector, i.e., $\Phi_B = (k-\beta)z = (k-\sqrt{k^2-k_r^2})z$ [26].

Figures 2(a) and 2(b) depict the Gouy phases of these two kinds of beams with different transverse parameters versus the propagation distance, respectively. Here, the parameters shown in Fig. 2(a) correspond to zeroth-order ($l = 0$) Bessel beams with different transverse wave vectors. Clearly, for a Bessel beam, the Gouy phase linearly accumulates with the increase of propagation distance, whose gradient is proportional to its

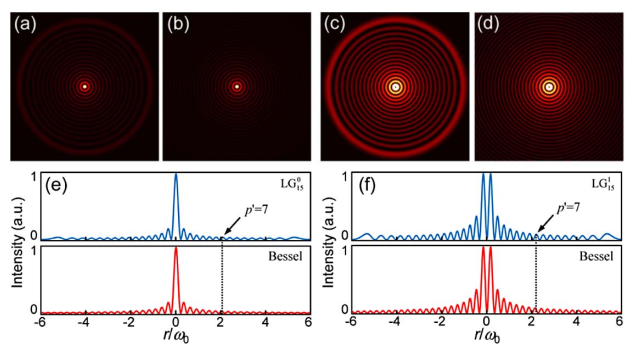

Fig. 1. Comparison of intensity distributions of higher-radial-order LG beams and their corresponding Bessel beams. (a), (b) $l = 0$, $p = 15$. (c), (d) $l = 1$, $p = 15$. (e), (f) Comparisons of intensity distributions of the LG (blue lines) and Bessel (red lines) beams along the radial direction. The dotted black lines in (e) and (f) depict the similarity of intensity profiles.

transverse wave vector, i.e., the equivalent parameter. In comparison, Fig. 2(b) shows the Gouy phases of LG beams with 15th-order radial index, i.e., $p = 15$, but variant topological charges. These significantly different Gouy phases intuitively indicate that these two kinds of beams have obvious birefringence in free space. To obtain a generic model, under the precondition of intensity profile, we set $l_1 = \pm l_2 = l$; the Gouy phase difference thus can be expressed as

$$\Delta\Phi(z) = \left(k - \sqrt{k^2 - k_r^2}\right)z - (2p + |l| + 1)\arctan\left(\frac{z}{z_R}\right). \tag{4}$$

Supposing that the LG and Bessel beams have right- and left-handed circular polarizations, i.e., $|\mathrm{R}\rangle$ and $|\mathrm{L}\rangle$ states, respectively, so that the superimposed beam presents a superposition state expressed as $\mathbf{E}(z) = \mathbf{E}_{\mathrm{LG}}(z) + \mathbf{E}_B(z) \approx E_B|\mathrm{R}\rangle + \exp[i\Delta\Phi(z)]|\mathrm{L}\rangle$, where E_B denotes the complex amplitude of the Bessel component. Clearly, the z-dependent Gouy phase difference produces longitudinally variant polarization. To intuitively observe the polarization transformation induced by Gouy phase, we map the trajectory on the Poincaré sphere, as shown in Fig. 2(c). On this Poincaré sphere, the superposition state with respect to two spin polarizations is located on the equator with longitude angle equal to $\Delta\Phi$, and the corresponding linear polarization orientation is $\theta = \Delta\Phi/2$. Therefore, with the increase of Gouy phase difference of two component beams, the superimposed beam rotates its polarization, with an angular velocity expressed as

$$\omega = \frac{\partial}{\partial z}\theta(z) = \left(k - \sqrt{k^2 - k_r^2}\right)/2 - N\frac{z_R}{z_R^2 + z^2}, \tag{5}$$

from which we instantly find the angular acceleration as follows:

$$\beta = \frac{\partial}{\partial z}\omega(z) = \frac{2Nz_R z}{(z_R^2 + z^2)^2}. \tag{6}$$

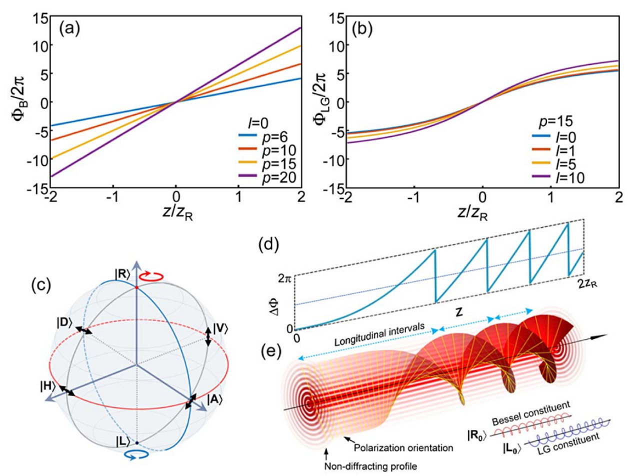

Fig. 2. (a), (b) Gouy phases of Bessel and LG beams with different transverse parameters, respectively. (c) Canonical Poincaré sphere. (d) Gouy phase difference between LG_{15}^0 beam and its corresponding zeroth-order Bessel beam versus propagation distance. (e) Gouy phase-induced self-accelerated OA of zeroth-order superimposed beam.

According to Eqs. (4)–(6), we find that the superimposed beam rotates its polarization at a non-constant angular velocity and also a non-constant angular acceleration, which strongly depend on the transverse mode parameters, i.e., l and p.

Figure 2(d) displays the z-dependent Gouy phase difference of an LG_{15}^0 beam and the corresponding zeroth-order Bessel beam. Here, the LG_{15}^0 beam and Bessel beam have left and right spin polarizations, respectively, i.e., the $|\mathrm{L}_0\rangle$ and $|\mathrm{R}_0\rangle$ states. As a result, the rotation direction of the OA is clockwise along the equator on the Poincaré sphere upon beam propagation, as the red trajectory mapped in Fig. 2(c). The corresponding OA of a zeroth-order non-diffracting beam is schematically shown in Fig. 2(e). It is worth noting that the rotation direction of the OA is tunable by exchanging the spin polarizations of two component beams. Furthermore, the basic states of the LG and Bessel components can be defined as any pair of orthogonal polarizations on the Poincaré sphere. As a result, it is possible to control the polarization trajectory as any great circle, e.g., the blue meridian mapped in Fig. 2(c). In addition, from results shown in Figs. 2(a), 2(b), and 2(d), we can find that, in theory, the z-dependent Gouy phase difference decelerates, close to linear accumulation; that is, the accelerating effect disappears when the propagation distance is great enough.

3. EXPERIMENT AND RESULTS

Figure 3 reports the experimental setup. A linearly polarized laser ($\lambda = 532$ nm) passing through a half-wave plate is expanded, collimated, and then orderly input into a beam splitter (BS) and a polarized beam splitter (PBS). Two orthogonally polarized beams output from the PBS are incident onto two identical reflective-type spatial light modulators (SLMs, HOLOEYE, Pluto, 1920 × 1280 pixels), which upload computer-generated holograms to generate the LG and Bessel components. Two reflected beams are then coaxially reproduced by the PBS and orderly pass through the BS and a $4f$ filter system consisting of two lenses, a quarter-wave plate (QWP), and a filter, which allows only two +1st-order diffraction components to pass through. The inset QWP in the $4f$ filter system is used to transform two linearly polarized components into circular polarizations or other orthogonal polarizations. Nearby the back focal plane of the $4f$ filter system, a CCD

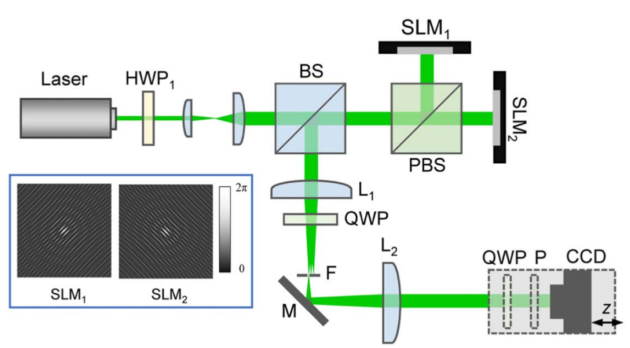

Fig. 3. Experimental setup. HWP, half-wave plate; BS, beam splitter; PBS, polarized beam splitter; SLM, spatial light modulator; QWP, quarter-wave plate; L, lens; F, filter; M, mirror; P, polarizer. Insets: computer-generated holograms.

camera placed on a linear stage is used to three-dimensionally (3D) observe the output field. The QWP and polarizer denoted by the dashed graphs are combined to measure the superposition state. The insets show the holograms loaded onto the SLMs. It should be noted that, because of the aperture effect of the SLM and the finite waist of incident beam, the output beams actually present quasi-Bessel patterns and non-diffracting propagation in a finite distance.

Initially, we demonstrate the self-accelerated OA of a scalar quasi-non-diffracting beam, i.e., $l_1 = l_2 = 0$, of which the OA has a rotation dynamic as shown in Fig. 2(e). In experiment, the azimuthal and radial indices of the LG component are $l = 0$ and $p = 15$, respectively. For such a case, $N = 15.5$, the corresponding zeroth-order Bessel component has a transverse wave vector of $k_r = 44869\ \text{m}^{-1}$. Figure 4(a) shows the measured intensity distribution of the superimposed beam consisting of these LG and Bessel components in a 3D space. It can be seen that, on the whole, the beam keeps its intensity profile in a long distance. In other words, it presents non-diffracting property in this interval. The inset white dashed lines correspond to two special planes, where $\Delta\Phi = \pi$ and 2π, respectively. In practice, we set $\Delta\Phi = 0$ at the $z = 0$ (z_0) plane, so that the output superimposed beam has a horizontal polarization, i.e., $\theta = 0$.

Figure 4(b) displays the intensity distributions of the total field, horizontal and vertical components at the z_0, z_1, and z_2 planes, respectively. As shown by results, this scalar quasi-non-diffracting beam has an initial $|\mathrm{H}\rangle$ state, and then orderly transforms its state along a circle of $|\mathrm{H}\rangle \to |\mathrm{V}\rangle \to |\mathrm{H}\rangle$ within inequivalent intervals, validating the rotation effect of polarization. Note that, for the LG beam having quasi-Bessel propagating behavior, its non-diffracting distance is directly proportional to the efficient radius R_0, i.e., $z_{\max} \approx R_0/2\ \tan\,\alpha$, with

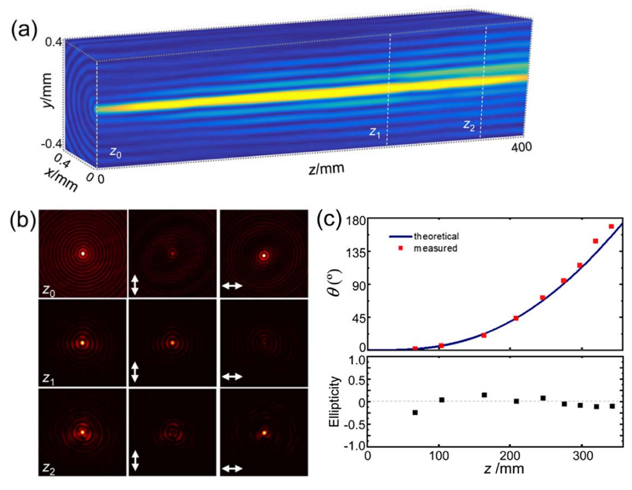

Fig. 4. Self-accelerated OA of a scalar (zeroth-order) quasi-non-diffracting beam. (a) 3D intensity profile of light field composed by an LG_{15}^{0} component and a corresponding Bessel component. (b) Intensity distributions of total field, horizontal, and vertical components at the z_0, z_1, and z_2 planes. The white arrows denote the orientation of polarizer. (c) Upper graph: comparison of theoretically calculated (blue curve) and measured (red squares) polarization orientations; below graph: measured polarization ellipticities. Both are the measured results on the axis.

$\sin\,\alpha = k_r/k$. Here, for such experimental parameters, the non-diffracting distance is slightly larger than z_R, fulfilling an OA period. To achieve more OA periods, we can enhance the non-diffracting distance by increasing the radial index.

The self-accelerated property is evident from Fig. 4(c), which reports the measured polarization state on the axis in a period of OA. In the upper graph, the red squares and blue curve correspond to the detected and prospective polarization orientations, respectively. The below graph depicts the measured polarization ellipticities. The experimental results are calculated according to the Stokes parameter method. The measured data are consistent with the theoretical predictions, that is, the polarization state automatically varies along the expected trajectory on the Poincaré sphere with prospective self-accelerated property. As shown in the aforementioned theory, when $\omega \cdot \beta > 0$, the angular velocity increases with z, which can be intuitively observed from the gradient of rotation angle shown in Fig. 4(c). Furthermore, it should be noted that, because the practically generated Bessel component has a Gaussian-like intensity profile along the z direction [32], the polarization ellipticity of the quasi-non-diffracting beam actually appears with a perturbation, whose profile is similar to the z-dependent intensity profile of the Bessel component.

Next, we consider the self-accelerated OA of vector quasi-non-diffracting beams. For such cases, the LG and Bessel components have non-zero azimuthal indices, i.e., $l_1 = -l_2 \neq 0$. So the superimposed beam presents azimuthally variant polarization, namely, vector mode [33], of which the azimuthal variation of polarization can be depicted by the polarization order m. To intuitively describe the polarization structures, high-order and hybrid Poincaré spheres have been proposed [34,35], as shown in Fig. 5(a), whose poles depict spatial modes with homogenous spin polarizations but non-zero OAMs. Here, as an example, we set two components that have opposite first-order vortices and spin polarizations, i.e., $l_1 = 1$ and $l_2 = -1$, respectively. The corresponding states are denoted as $|\mathrm{L}_{+1}\rangle$ and $|\mathrm{R}_{+1}\rangle$, respectively. Consequently, the superimposed beam has a vector mode with a parameter of $m = l_1 = 1$. Four typical vector modes with locally linear polarization are depicted on the equator of this first-order Poincaré sphere, as shown in Fig. 5(a). The insets display the local polarization direction of such modes. It is crucial to note that the LG and Bessel components have not exactly the same intensity profiles, but within the $p' < p/2$ rings, polarizations are radially homogeneous.

For a vector beam with azimuthally variant polarization, i.e., $m \neq 0$, Eqs. (4)–(6) can only describe the OA of local polarization separately [36,37]. However, as shown in Fig. 5(b), the rotation of local polarization presents an overall effect at the transverse plane, as the transformation of the polarization mode. We therefore need to define corresponding parameters to represent this overall effect induced by the Gouy phase, because this overall effect can be described by the transformation of the polarization mode [38,39], with an intuitive trajectory mapped on the higher-order Poincaré sphere. We decompose the polarization mode as a superposition state with respect to the horizontal and vertical polarizations, i.e., the $|\mathrm{H}\rangle$ or $|\mathrm{V}\rangle$ states. Significantly, as shown in the inset of Fig. 5(b), the

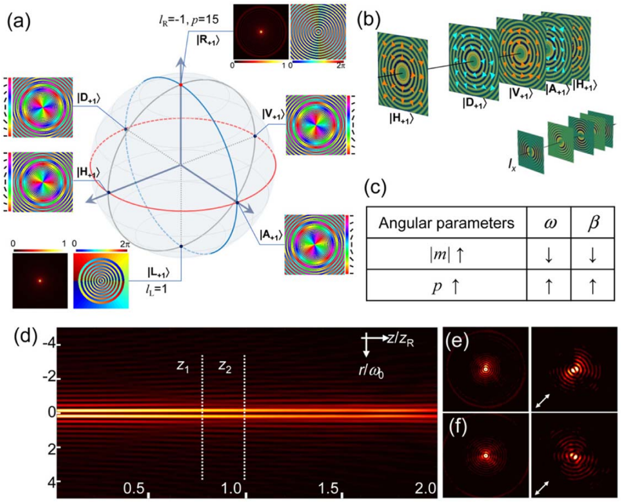

Fig. 5. Self-accelerated OA of vector non-diffracting beams. (a) Higher-order Poincaré sphere composed by two kinds of quasi-non-diffracting components carrying OAMs. Insets: $|\mathrm{R}_{+1}\rangle$ and $|\mathrm{L}_{+1}\rangle$, intensity and phase distributions; $|\mathrm{H}_{+1}\rangle$, $|\mathrm{A}_{+1}\rangle$, $|\mathrm{V}_{+1}\rangle$, and $|\mathrm{D}_{+1}\rangle$, polarization orientation distributions of four typical vector modes on the equator. (b) Schematic polarization transformation of vector non-diffracting beam and the corresponding rotation of petal-like intensity (horizonal component I_x). Arrows: local polarization orientations. (c) Correlation of rotation angular parameters and spatial mode indices. (d) Calculated intensity distribution in the y–z plane. (e), (f) Measured intensity distributions of the total and diagonal components at the z_1 and z_2 planes.

linearly polarized component has an impressive petal-like intensity profile relevant to the polarization order m. Therefore, we here use the rotation of this petal-like intensity profile to describe the overall effect induced by the Gouy phase [40], that is, the self-accelerated OA of a vector non-diffracting beam. So, the rotation angle can be rewritten as

$$\theta = \frac{1}{2|m|}\left[\left(k - \sqrt{k^2 - k_r^2}\right)z - 2N\ \arctan\left(\frac{z}{z_R}\right)\right]. \tag{7}$$

The angular velocity and acceleration of the rotation thus can be rewritten as

$$\omega = \frac{1}{2|m|}\left[\left(k - \sqrt{k^2 - k_r^2}\right) - 2N\frac{z_R}{z_R^2 + z^2}\right],$$
$$\beta = \frac{2N z_R z}{|m|(z_R^2 + z^2)^2}. \tag{8}$$

Clearly, the rotation directly depends on the polarization order m. Moreover, the parameter N affects closely the self-accelerating rotation. This means that by modulating the radial index p, it is also possible to control the self-accelerated OA. According to Eq. (8), we can point out that the rotation angle and angular acceleration are inversely proportional to the polarization order m but proportional to the radial index p, as the description in the diagram of Fig. 5(c).

Figure 5(d) shows the simulated intensity distribution of the first-order vector quasi-non-diffracting beam in the y–z plane with parameters of $l = 1$ and $p = 15$. Figures 5(e) and 5(f) display the measured total intensity and diagonal component at the z_1 and z_2 planes, respectively. In the interval of z_1 and z_2, the Gouy phase difference increases π, i.e., $\Delta\Phi(z_2) - \Delta\Phi(z_1) = \pi$. As is known, one issue of critical importance of the LG beam with zeroth radial index is the divergence that the beam enlarges during propagation with divergence angle, which is strongly dependent on its topological charge. Here, it is observed that the LG component keeps well intensity profile during beam propagating in such a distance. In addition, as expected, the petal-like intensity profile rotates $\pi/2$.

Figure 6 reports the comparison of theoretical and experimental results about the self-accelerated OA of vector quasi-non-diffracting beams with different polarization orders. In this diagram, the intensity distributions of the vertical component in several sliced planes are shown as backgrounds; the rotated white lines and angle values depict the theoretical rotation angles that are calculated from Eq. (7). Overall, the experimental and theoretical results are in good agreement. In Fig. 6, the first row shows a first-order vector beam, i.e., $m = 1$, since it is composed by an LG_{15}^{-1} component with $|\mathrm{R}\rangle$ state and an $l_2 = 1$ Bessel component with $|\mathrm{L}\rangle$ state. The increase of Gouy phase difference between these two spin components leads to the superposition state rotating anticlockwise along the equator on the first-order Poincaré sphere. Intuitively, the dipole-like intensity profile rotates in a clockwise direction. As shown, it rotates −20° after propagating 15.5 cm, while the rotation angle increases another 20° just in the next 4 cm. Clearly, the angular velocity accelerates as the increase of z, but verges on a maximum value. The second row corresponds to a second-order vector beam that consists of an LG_{15}^{-2} component with $|\mathrm{R}\rangle$ state and an $l_2 = 2$ Bessel component with $|\mathrm{L}\rangle$ state. As expected, the rotation velocity and acceleration both are lower than those of the first-order vector beam. Moreover, it should be noted that, for the vector beam with polarization order $m < 0$, the petal-like pattern rotates along the opposite direction. This means that, besides exchanging the spin states of two components, we can also control the direction of angular velocity and acceleration by exchanging the topological charge signs.

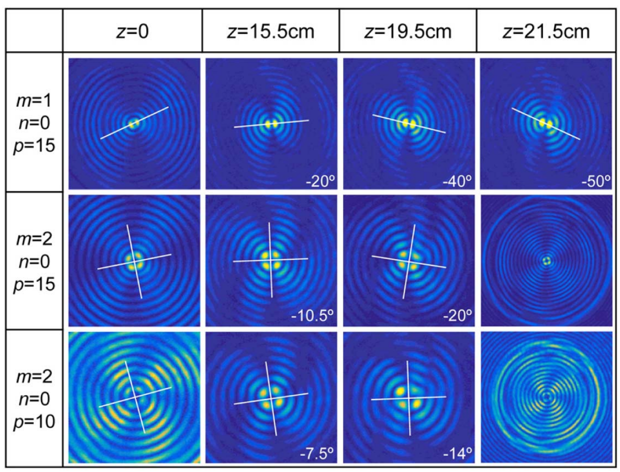

Fig. 6. Self-accelerated OA of different vector quasi-non-diffracting beams. Backgrounds: intensity distributions of the vertical component; white lines and values denote the theoretical rotation angles.

Furthermore, we demonstrate the dependence on the radial index. The compared results about second-order quasi-non-diffracting beams with different radial indices are shown in the two bottom rows in Fig. 6, where the last column depicts the total intensity patterns of two vector fields. As theoretical prediction, angular parameters are proportional to the radial index. Significantly different from the OA induced by two Bessel beams, this kind of quasi-non-diffracting beam rotates its polarization but keeps well intensity distribution. As shown in the experimental results, clear bright rings always can be observed during propagation, which means that the field has uniform polarization ellipticity along the radial direction in such ring regions.

These results demonstrate the controllability of this kind of self-accelerated OA, including angular velocity, acceleration, and transformation trajectory. One of the experimental limitations is the fact that Bessel and LG beams cannot be created with infinite amounts of energy, because the SLM actually plays the role of the aperture, which leads to the decrease of the amount of OA period. Furthermore, in the aforementioned experimental realization, the OA periods are in the scale of tens of centimeters. For better realization, greater angular acceleration requires a bigger N; in other words, the LG beam should have more rings. Inevitably, there is also a problem about the aperture in experimental realization.

4. CONCLUSIONS

We have theoretically and experimentally studied the self-accelerated OA within scalar and vector quasi-non-diffracting beams induced by the Gouy phase in free space. Moreover, we discussed the dependence of rotation on the spatial parameters, including azimuthal and radial indices. The results show that the rotation of a scalar beam depends on the mode parameters of the LG component. The rotation of a vector beam is mainly related to its polarization order, so that the vector beam with higher polarization order presents lower rotation velocity and acceleration, but higher radial order enhances the rotation. It not only demonstrates this intrinsic phenomenon, but more fundamentally, reveals an original scenario that could be further investigated in other waves.

Funding. National Natural Science Foundation of China (11634010, 11774289, 61675168, 91850118); National Key Research and Development Program of China (2017YFA0303800); Joint Fund of the National Natural Science Foundation of China and the China Academy of Engineering Physics (U1630125); Fundamental Research Funds for the Central Universities (3102018zy036, 3102019JC008); Seed Foundation of Innovation and Creation for Graduate Students in Northwestern Polytechnical University (ZZ2019220).

Disclosures. The authors declare no conflicts of interest.

REFERENCES

1. P. Yu, J. Li, C. Tang, H. Cheng, Z. Liu, Z. Li, Z. Liu, C. Gu, J. Li, S. Chen, and J. Tian, "Controllable optical activity with non-chiral plasmonic metasurfaces," Light Sci. Appl. **5**, e16096 (2016).
2. E. Plum, X. X. Liu, V. A. Fedotov, Y. Chen, D. P. Tsai, and N. I. Zheludev, "Metamaterials: optical activity without chirality," Phys. Rev. Lett. **102**, 113902 (2009).
3. Q. Zhan, "Cylindrical vector beams: from mathematical concepts to applications," Adv. Opt. Photonics **1**, 1–57 (2009).
4. X. Wang, J. Chen, Y. Li, J. Ding, C. Guo, and H. Wang, "Optical orbital angular momentum from the curl of polarization," Phys. Rev. Lett. **105**, 253602 (2010).
5. M. Zhong, L. Gong, D. Li, J. Zhou, Z. Wang, and Y. Li, "Optical trapping of core-shell magnetic microparticles by cylindrical vector beams," Appl. Phys. Lett. **105**, 181112 (2014).
6. G. Milione, M. P. J. Lavery, H. Huang, Y. Ren, G. Xie, T. A. Nguyen, E. Karimi, L. Marrucci, D. A. Nolan, R. R. Alfano, and A. E. Willner, "4×20 Gbit/s mode division multiplexing over free space using vector modes and a q-plate mode (de)multiplexer," Opt. Lett. **40**, 1980–1983 (2015).
7. X. Gao, Y. Pan, S. Li, D. Wang, Y. Li, C. Tu, and H. Wang, "Vector optical fields broken in the spatial frequency domain," Phys. Rev. A **93**, 033834 (2016).
8. R. D. Halina, F. Andrew, M. V. Berry, M. R. Dennis, L. A. David, M. Masud, D. Cornelia, A. Christina, B. Peter, B. Thomas, K. Ebrahim, M. Lorenzo, P. Miles, R.-M. Monika, M. L. Natalia, P. B. Nicholas, C. Rosales-Guzmán, A. Belmonte, J. P. Torres, W. N. Tyler, B. Mark, G. Reuven, B. S. Alexander, R. Jacquiline, G. W. Andrew, F. Robert, E. W. Alan, X. Guodong, M. Benjamin, and M. W. Andrew, "Roadmap on structured light," J. Opt. **19**, 013001 (2017).
9. J. Wang, X. Yang, Y. Li, Y. Chen, M. Cao, D. Wei, H. Gao, and F. Li, "Optically spatial information selection with hybridly polarized beam in atomic vapor," Photon. Res. **6**, 451–456 (2018).
10. B. Gu, B. Wen, G. Rui, Y. Xue, Q. Zhan, and Y. Cui, "Varying polarization and spin angular momentum flux of radially polarized beams by anisotropic Kerr media," Opt. Lett. **41**, 1566–1569 (2016).
11. B. Wei, S. Qi, S. Liu, P. Li, Y. Zhang, L. Han, J. Zhong, W. Hu, Y. Lu, and J. Zhao, "Auto-transition of vortex- to vector-Airy beams via liquid crystal q-Airy-plates," Opt. Express **27**, 18848–18857 (2019).
12. I. Moreno, J. A. Davis, M. M. Sánchez-López, K. Badham, and D. M. Cottrell, "Nondiffracting Bessel beams with polarization state that varies with propagation distance," Opt. Lett. **40**, 5451–5454 (2015).
13. P. Li, Y. Zhang, S. Liu, L. Han, H. Cheng, F. Yu, and J. Zhao, "Quasi-Bessel beams with longitudinally varying polarization state generated by employing spectrum engineering," Opt. Lett. **41**, 4811–4814 (2016).
14. J. A. Davis, I. Moreno, K. Badham, M. M. Sánchez-López, and D. M. Cottrell, "Nondiffracting vector beams where the charge and the polarization state vary with propagation distance," Opt. Lett. **41**, 2270–2273 (2016).
15. S. Fu, S. Zhang, and C. Gao, "Bessel beams with spatial oscillating polarization," Sci. Rep. **6**, 30765 (2016).
16. P. Li, D. Wu, Y. Zhang, S. Liu, Y. Li, S. Qi, and J. Zhao, "Polarization oscillating beams constructed by copropagating optical frozen waves," Photon. Res. **6**, 756–761 (2018).
17. S. Liu, S. Qi, P. Li, B. Wei, P. Chen, W. Hu, Y. Zhang, X. Gan, P. Zhang, Y. Lu, Z. Chen, and J. Zhao, "Optically active beams: non-reciprocal optical activity in free space induced by spin-orbital interaction of light," arXiv:1908.10008 (2019).
18. M. Duocastella and C. B. Arnold, "Bessel and annular beams for materials processing," Laser Photonics Rev. **6**, 607–621 (2012).
19. G. Guzzinati, P. Schattschneider, K. Y. Bliokh, F. Nori, and J. Verbeeck, "Observation of the Larmor and Gouy rotations with electron vortex beams," Phys. Rev. Lett. **110**, 093601 (2013).
20. T. C. Petersen, D. M. Paganin, M. Weyland, T. P. Simula, S. A. Eastwood, and M. J. Morgan, "Unifying interpretations of the Gouy phase anomaly for electron waves," Phys. Rev. A **89**, 063801 (2014).
21. R. Ducharme and I. G. da Paz, "Gouy phase for relativistic quantum particles," Phys. Rev. A **92**, 023853 (2015).
22. L. Allen, M. W. Beijersbergen, R. J. C. Spreeuw, and J. P. Woerdman, "Orbital angular momentum of light and the transformation of Laguerre–Gaussian laser modes," Phys. Rev. A **45**, 8185–8189 (1992).
23. J. Mendoza-Hernández, M. L. Arroyo-Carrasco, M. D. Iturbe-Castillo, and S. Chávez-Cerda, "Laguerre–Gauss beams versus Bessel

beams showdown: peer comparison," Opt. Lett. **40**, 3739–3742 (2015).
24. A. Rubinowicz, "On the anomalous propagation of phase in the focus," Phys. Rev. **54**, 931–936 (1938).
25. Z. Derrar Kaddour, A. Taleb, K. Ait-Ameur, and G. Martel, "Revisiting Gouy phase," Opt. Commun. **280**, 256–263 (2007).
26. P. Martelli, M. Tacca, A. Gatto, G. Moneta, and M. Martinelli, "Gouy phase shift in nondiffracting Bessel beams," Opt. Express **18**, 7108–7120 (2010).
27. S. Feng and H. G. Winful, "Physical origin of the Gouy phase shift," Opt. Lett. **26**, 485–487 (2001).
28. M. Neugebauer, S. Grosche, S. Rothau, G. Leuchs, and P. Banzer, "Lateral spin transport in paraxial beams of light," Opt. Lett. **41**, 3499–3502 (2016).
29. Y. Zhang, X. Guo, L. Han, P. Li, S. Liu, H. Cheng, and J. Zhao, "Gouy phase induced polarization transition of focused vector vortex beams," Opt. Express **25**, 25725–25733 (2017).
30. M. M. Sánchez-López, J. Davis, I. Moreno, A. Cofré, and D. Cottrell, "Gouy phase effects on propagation of pure and hybrid vector beams," Opt. Express **27**, 2374–2386 (2019).
31. A. A. Tovar, "Production and propagation of cylindrically polarized Laguerre–Gaussian laser beams," J. Opt. Soc. Am. A **15**, 2705–2711 (1998).
32. T. Čižmár and K. Dholakia, "Tunable Bessel light modes: engineering the axial propagation," Opt. Express **17**, 15558–15570 (2009).
33. P. Li, Y. Zhang, S. Liu, C. Ma, L. Han, H. Cheng, and J. Zhao, "Generation of perfect vectorial vortex beams," Opt. Lett. **41**, 2205–2208 (2016).
34. G. Milione, H. I. Sztul, D. A. Nolan, and R. R. Alfano, "Higher-order Poincaré sphere, stokes parameters, and the angular momentum of light," Phys. Rev. Lett. **107**, 053601 (2011).
35. X. Yi, Y. Liu, X. Ling, X. Zhou, Y. Ke, H. Luo, S. Wen, and D. Fan, "Hybrid-order Poincaré sphere," Phys. Rev. A **91**, 023801 (2015).
36. G. M. Philip, V. Kumar, G. Milione, and N. K. Viswanathan, "Manifestation of the Gouy phase in vector-vortex beams," Opt. Lett. **37**, 2667–2669 (2012).
37. F. Cardano, E. Karimi, L. Marrucci, C. de Lisio, and E. Santamato, "Generation and dynamics of optical beams with polarization singularities," Opt. Express **21**, 8815–8820 (2013).
38. P. Li, Y. Zhang, S. Liu, H. Cheng, L. Han, D. Wu, and J. Zhao, "Generation and self-healing of vector Bessel–Gauss beams with variant state of polarizations upon propagation," Opt. Express **25**, 5821–5831 (2017).
39. B. Gu, Y. Pan, G. Rui, D. Xu, Q. Zhan, and Y. Cui, "Polarization evolution characteristics of focused hybridly polarized vector fields," Appl. Phys. B **117**, 915–926 (2014).
40. C. Schulze, F. S. Roux, A. Dudley, R. Rop, M. Duparré, and A. Forbes, "Accelerated rotation with orbital angular momentum modes," Phys. Rev. A **91**, 043821 (2015).